

ASTRONOMICAL IMAGE DECONVOLUTION USING SPARSE PRIORS: AN ANALYSIS-BY-SYNTHESIS APPROACH

A. Dabbech, D. Mary,*

C. Ferrari,

Lab. Fizeau, UNSA, OCA, UMR CNRS 6525,
Parc Valrose, 06108 Nice, France

Lab. Cassiopée, OCA, UMR CNRS 6202,
B.P. 4229, 06304 Nice Cedex, France

ABSTRACT

This paper deals with the deconvolution of faint diffuse astronomical sources buried in the PSF sidelobes of surrounding bright compact sources, and in the noise. We propose a sparsity promoting restoration model which is based on highly redundant, shift invariant dictionaries, and which is hybrid in its sparsity priors. On one hand, the image to be restored is modelled using sparse *synthesis* priors as a sum of few atoms (objects) which, as opposed to classical synthesis-based priors, are unknown. On the other hand, these objects are iteratively estimated and deconvolved through *analysis*-based priors. The faint diffuse source is deconvolved once the data has been cleaned from all brighter sources' contributions. Comparative numerical results show that the method is efficient and fast.

Index Terms— Sparse priors, Analysis, Synthesis, Deconvolution, Wavelets

1. INTRODUCTION: DATA MODEL AND SPARSE PRIORS

A new generation of radio interferometers (LOFAR, ASKAP, MeerKAT, ...) are being built as instrumental and scientific pathfinders of the world's largest radio telescope, the Square Kilometre Array. Thanks to the exploitation of massive computing, dedicated signal processing, innovative antenna design, and to the consequent increase both of their bandwidth and of their instantaneous field of view, these instruments will allow to survey the sky at unprecedented sensitivity and resolution in a wide region of the radio band. Surely with these telescopes will come new astrophysical science, but new image processing challenges as well, in particular the ability of restoration algorithms to recover *faint and diffuse* radio sources.

In this paper, \mathbf{X} denotes a matrix, \mathcal{X} an operator, \mathbf{x} and \mathbf{X}_i (the i^{th} vector column of \mathbf{X}) are vectors, $x[k]$ is the k^{th} entry of \mathbf{x} , x and X are scalars. Without loss of generality, images are considered as vectors. With these notations, the data model in radiointerferometry reads [1]:

$$\mathbf{y} = \mathbf{F}^\dagger \mathbf{M}^\dagger \mathbf{W} \mathbf{M} \mathbf{F} \mathbf{x} + \mathbf{n} = \mathbf{H} \mathbf{x} + \mathbf{n}, \quad (1)$$

where $\mathbf{y} \in \mathbb{R}^N$ represents the data, also called *the dirty map*, \mathbf{F} is the Fourier transform and \mathbf{F}^\dagger its conjugate transpose, \mathbf{W} is an $N \times N$ diagonal weighting-matrix including various operations (calibration, signal to noise weighting), \mathbf{M} is an $N \times N$ diagonal matrix with ones and zeros on the diagonal, whose ones select available Fourier samples, $\mathbf{x} \in \mathbb{R}^{+N}$ is the unknown image of size N , $\mathbf{n} \in \mathbb{R}^N$ is the noise. This imaging system corresponds essentially to an optical linear filter whose transfer function is described by $\mathbf{W} \mathbf{M} \mathbf{F}$.

*We acknowledge financial support by the Agence Nationale de la Recherche through grant ANR-09-JCJC-0001-01. We also thank Matthew Whiting of the CSIRO ASKAP project for providing the point spread functions used in our work.

This transfer function has many zeros, making the problem of reconstructing \mathbf{x} from \mathbf{y} under-determined and ill-posed. The matrix $\mathbf{H} = \mathbf{F}^\dagger \mathbf{M}^\dagger \mathbf{W} \mathbf{M} \mathbf{F}$ corresponds to a convolution, with a shifted version of the Point Spread Function (PSF) as each of its columns. In radiointerferometry, the PSF has typically numerous, slowly decreasing sidelobes due to the sparse sampling of the Fourier-space. This makes the recovery of faint objects particularly difficult when surrounding sources are orders of magnitude brighter.

In this framework, satisfying restoration methods must use *a priori* knowledge on \mathbf{x} , such as positivity or information about the geometry of the image. Besides, the restoration algorithms used in radioastronomy cannot have arbitrary computational costs, as the considered images have millions of pixels. The problem of restoring faint diffuse sources which are submerged by the contribution of the sidelobes of brighter sources has lead us to a fast restoration method which exploits positivity, and sparse priors in a hybrid manner.

Considering model (1), where \mathbf{n} is assumed for now to be an independent and identically distributed (i.i.d.), zero-mean, unit variance white Gaussian noise, sparsity-promoting models can build on two kinds of priors: synthesis and analysis [2].

In the synthesis approach, the solution \mathbf{x} is sparsely synthesized by atoms of a given full rank dictionary \mathbf{S} of size (N, L) : \mathbf{x} is written as $\mathbf{x} = \mathbf{S} \boldsymbol{\gamma}$, where $\boldsymbol{\gamma}$ (the synthesis coefficients vector) is sparse. The sparse synthesis solution \mathbf{x}_S^* , also interpretable as a Maximum A Posteriori (MAP) solution, is obtained by:

$$\mathbf{x}_S^* = \mathbf{S} \cdot \{\arg \min_{\boldsymbol{\gamma}} \frac{1}{2} \|\mathbf{H} \mathbf{S} \boldsymbol{\gamma} - \mathbf{y}\|^2 + \mu_p \|\boldsymbol{\gamma}\|_p^p\}, \quad (2)$$

where μ_p is a hyper parameter that tunes the *a priori* penalty (μ_p is related in the MAP framework to the parameters of a Generalized Gaussian prior on $\boldsymbol{\gamma}$). The l^0 quasi-norm is the most natural sparsity measure. Yet, to ensure the convexity of the resulting cost function, it is often replaced by the l^1 norm $\|\cdot\|_1$, which still promotes sparsity and correspond to a Laplacian prior on $\boldsymbol{\gamma}$.

In contrast, the analysis approach consists in finding the solution \mathbf{x} that is not correlated with some atoms of a dictionary \mathbf{A} of size (N, L) : $\mathbf{A}^T \mathbf{x}$ is sparse. The sparse analysis solution is:

$$\mathbf{x}_A^* = \arg \min_{\mathbf{x}} \frac{1}{2} \|\mathbf{H} \mathbf{x} - \mathbf{y}\|^2 + \mu_p \|\mathbf{A}^T \mathbf{x}\|_p^p. \quad (3)$$

Note that the synthesis prior is on the synthesis coefficients $\boldsymbol{\gamma}$, while the analysis one is on the projection $\mathbf{a} = \mathbf{A}^T \mathbf{x}$ of the signal on an analysis dictionary \mathbf{A} .

While both approaches are equivalent when \mathbf{A} and \mathbf{S} are square and invertible, with $\mathbf{A} = \mathbf{S}^{-1}$, they yield in general different solutions for overcomplete dictionaries ($N < L$) - which are required for efficient image restoration [2]. Since natural images can be approximated by few atomic elements in such dictionaries, the synthesis approach is considered as more intuitive. Its design simplicity

(in greedy approaches) has also made it more popular in image processing applications. However, the solution is restricted to a column subspace of the synthesis dictionary, so that the significance of each selected atom is important. On the other hand, the analysis approach may be more robust to false detections since the signal is not built from a few number of atoms [2]. The present paper does not intend to investigate how the two approaches compare, but rather proposes a method mixing both approaches.

For large images, greedy approaches are often preferred to optimization methods solving (2) or (3), thanks to their lower complexity. In classical greedy approaches (typically CLEAN [3] in radio interferometry - an algorithm similar to the Matching Pursuit, using \mathbf{H} as a dictionary of shifted PSFs- and its multiresolution variants), selection or removal of atoms is done one by one. These approaches have the capability of progressively revealing faint features initially buried in the contribution of brighter elements. However, for images with millions of pixels and even more analysis and synthesis coefficients, they can be very time-consuming.

These considerations have led us to consider an approach that consists in analysing the data with a highly redundant dictionary adapted to astronomical images (Isotropic Undecimated Wavelet Transform, IUWT, Sec. 2), and localizing the sparse significant analysis coefficients by packets. Each object assigned to a set of significant analysis coefficients is then deconvolved and subtracted in a synthesis manner. The deconvolved objects are thus considered as atoms that are estimated from the data (Sec. 3).

2. ISOTROPIC UNDECIMATED WAVELET TRANSFORM

The IUWT [4] presents interesting features for the considered problem. First, its adaptability to astronomical objects, since most of them are quasi isotropic (stars, galaxies, galaxy clusters...). Second, its rapidity as a transform. Third, the non decimation of the IUWT guarantees a fine modelling through its translation invariance.

2.1. Analysis and Synthesis with the IUWT

The IUWT decomposes an image of size N up to a level J into a set of analysis coefficients $\mathbf{a} = [\mathbf{w}_1^T, \dots, \mathbf{w}_J^T, \mathbf{c}_J^T]^T$, where \mathbf{c}_J is the smoothest approximation of the original image and \mathbf{w}_j are the detail coefficients sets at the scale indexes $j = 1, \dots, J$ (the indexing is such that $j = 1$ represents the highest frequencies).

An efficient way to obtain \mathbf{a} is to use the *à trous* algorithm [5]. Starting from the original image as the initial approximation coefficients set $\mathbf{c}_0 = \mathbf{x}$, the approximation and detail coefficients can respectively be obtained iteratively by:

$$\mathbf{c}_{j+1}[k] = \sum_m \mathbf{h}[m] \mathbf{c}_j[k + m2^j] = (\bar{\mathbf{h}}^{(j)} * \mathbf{c}_j)[k], \quad (4)$$

$$\mathbf{w}_{j+1}[k] = \sum_m \mathbf{g}[m] \mathbf{c}_j[k + m2^j] = (\bar{\mathbf{g}}^{(j)} * \mathbf{c}_j)[k]. \quad (5)$$

where $\bar{\mathbf{h}}^{(j)}[k]$ equals $\mathbf{h}[-k]$ if $k/2^j$ is integer and 0 otherwise, same for $\bar{\mathbf{g}}^{(j)}[k]$. The decomposition ends up with a vector \mathbf{a} of $(J+1)N$ analysis coefficients.

The reconstruction or synthesis of \mathbf{c}_0 from $\mathbf{a} = [\mathbf{w}_1^T, \dots, \mathbf{w}_J^T, \mathbf{c}_J^T]^T$ is obtained by the iterative recovery of each \mathbf{c}_j :

$$\mathbf{c}_j[k] = (\tilde{\mathbf{h}}^{(j)} * \mathbf{c}_{j+1})[k] + (\tilde{\mathbf{g}}^{(j)} * \mathbf{w}_{j+1})[k], \quad (6)$$

for $j = J-1, \dots, 0$, where $\tilde{\mathbf{h}}$ and $\tilde{\mathbf{g}}$ constitute the *synthesis* part of the filter bank.

The cascade analysis-synthesis guarantees perfect reconstruction if the filter bank $\{\mathbf{h}, \mathbf{g}, \tilde{\mathbf{h}}, \tilde{\mathbf{g}}\}$ verifies, in the z -transform domain, the condition: $H(z^{-1})\tilde{H}(z) + G(z^{-1})\tilde{G}(z) = 1$ (no anti-aliasing condition is required thanks to redundancy). In addition, the

filters should be i) *compact* since we are doing successive convolutions, ii) *regular* to avoid artifacts, iii) *even-symmetric* to guarantee the isotropy of the transform ($\mathbf{h} = \bar{\mathbf{h}}, \mathbf{g} = \bar{\mathbf{g}}$). Separability of the filters is not required but it allows fast computations since convolutions is then done successively on the rows and on the columns. The extension of the *à trous* algorithm above in two dimensions is in this case straightforward [5]. In [4], three different IUWT filter banks are exposed. In the results below, we focus on the filter bank called of "second generation" for which we obtained better results. In this bank, the synthesis atoms are positive and $\mathbf{h} = \tilde{\mathbf{h}}$. The high pass filter \mathbf{h} is derived from the B-spline function since it nearly satisfies the three conditions i)–iii) evoked above. The high pass analysis filter is $\mathbf{g} = \delta - \mathbf{h} * \mathbf{h}$, its corresponding synthesis filter is $\tilde{\mathbf{g}} = \delta$.

2.2. IUWT Filter bank : analysis and synthesis dictionaries

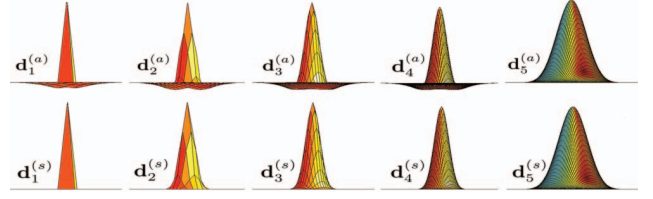


Fig. 1. Atoms of the analysis and synthesis dictionaries obtained by the considered IUWT filter bank for $J = 4$.

Reasoning now in terms of dictionaries, the IUWT analysis coefficients vector \mathbf{a} can be seen as $\mathbf{a} = [\mathbf{w}_1^T, \dots, \mathbf{w}_J^T, \mathbf{c}_J^T]^T = \mathbf{A}^T \mathbf{c}_0$, where \mathbf{A} is the IUWT analysis dictionary resulting from the filters $\{\mathbf{h}, \tilde{\mathbf{h}}, \mathbf{g}, \tilde{\mathbf{g}}\}$. \mathbf{A} can be written as $\mathbf{A} = [\mathbf{A}_{(1)}, \dots, \mathbf{A}_{(J+1)}]$, where each $\mathbf{A}_{(j)}$ is a sub-dictionary of size (N, N) , having shifted versions of the same analysis atom $\mathbf{d}_j^{(a)}$ at all pixels positions (Fig.1, top row). For instance, the analysis coefficients \mathbf{w}_1 correspond to N correlation coefficients of shifted versions of $\mathbf{d}_1^{(a)}$ with the original image. Equivalently, \mathbf{c}_0 can be recovered as $\mathbf{c}_0 = \mathbf{S} \mathbf{a}$, where $\mathbf{S} = [\mathbf{S}_{(1)}, \dots, \mathbf{S}_{(J+1)}]$, the $\mathbf{S}_{(j)}$ being sub-dictionaries of size (N, N) , whose columns are shifted versions of the synthesis atoms $\mathbf{d}_j^{(s)}$ (Fig.1, bottom row).

An example of analysis coefficients \mathbf{a} is shown in Fig. 2. Each astronomical object is associated to a set of few coefficients living at different scales (e.g., the small galaxy circled in green at the bottom right is visible mostly in small regions of scales $\mathbf{w}_2, \mathbf{w}_3, \mathbf{w}_4, \mathbf{c}_4$ - red circles). As a consequence, different objects can be identified and separated from the different "fingerprints" they leave on several scales. Below, objects will be denoted by \mathbf{X}_i and the corresponding "fingerprint" analysis coefficients by α_i . Clearly, each object leads to a sparse signature in the overall decomposition. The process of associating a small set of significant coefficients α_i to one object is called object identification below. Once identified, each such set of coefficients will be used to deconvolve the objects one by one.

3. ITERATIVE ANALYSIS-BY-SYNTHESIS APPROACH
An astronomical image \mathbf{x} can often be modelled as a sum of an unknown number P of objects \mathbf{X}_i (either compact or diffuse sources):

$$\mathbf{x} = \sum_{i=1}^P \mathbf{X}_i = \mathbf{X} \mathbf{1}_P, \quad (7)$$

where $\mathbf{X} = [\mathbf{X}_1, \dots, \mathbf{X}_P]$ can be seen as an unknown synthesis dictionary of size (N, P) , $P \ll N$ and $\mathbf{1}_P$ is a vector of P ones. The \mathbf{X}_i , columns of \mathbf{X} , are the positive unknown objects composing \mathbf{x} . With (7), the convolutive model (1) becomes :

$$\mathbf{y} = \mathbf{H} \mathbf{X} \mathbf{1}_P + \mathbf{n}, \text{ with } \mathbf{X} \in \mathbb{R}^{+N} \text{ and } P \ll N. \quad (8)$$

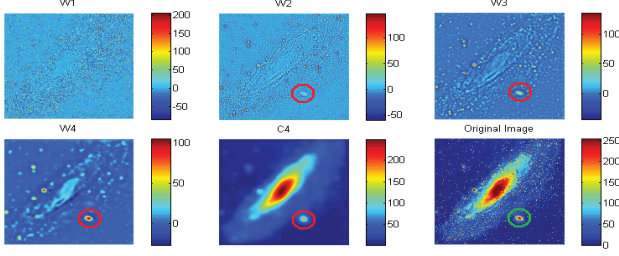


Fig. 2. IUWT analysis of Andromeda (bottom right) up to $J = 4$. The analysis coefficients circled in red correspond to the galaxy circled in green.

Model (8) is sparse in synthesis, since the image \mathbf{x} is reconstructed from few atoms \mathbf{X}_i . However, there are two differences with the sparse-synthesis model presented in Sec. 1. First, the atoms \mathbf{X}_i are unknown and must be estimated from the data. This estimation makes the task harder, but has the advantage that \mathbf{x} will not be restricted to a small column subspace of a generic dictionary. Second, the number of atoms P may be very small in comparison with the number of atoms of a generic dictionary which would be necessary to finely synthesize a real astronomical image. Thus, we save substantial computation time with this synthesis model.

When estimating the objects \mathbf{X}_i as well as their number P , care must be taken for faint large objects that are buried in the PSF lobes of the brighter objects. Deconvolution will thus be done in an iterative manner, at first on the brightest object whose contribution will be subtracted from the data, enabling the restitution of the faint object at last. To do this we need at each step an object identification strategy.

3.1. Object identification

To identify significant information related to the brightest object, we have opted for an object identification strategy inspired from [6]. First, the object identification is not done directly on \mathbf{a} , the noisy analysis coefficients of the data, but rather on a *significant analysis support* (SAS), that is, the support of those analysis coefficients that are significant with respect not only to noise, but also to convolution.

• *SAS with unknown noise level:* It is found in two steps. The first step is to determine which analysis coefficients are significant w.r.t. noise statistics. For an image composed of an i.i.d. Gaussian noise of standard deviation (s.d.) σ , the s.d. at each scale resolution σ_j is :

$$\sigma_j = \sigma \cdot \|\mathbf{d}_j^{(a)}\|, \quad (9)$$

where $\|\mathbf{d}_j^{(a)}\|$ is the l^2 norm of the analysis atom $\mathbf{d}_j^{(a)}$ of level j . Since the analysis coefficients set \mathbf{w}_1 contains the highest frequencies, σ can be estimated from σ_1 , the s.d. of \mathbf{w}_1 , by $\hat{\sigma} = \|\mathbf{d}_1^{(a)}\|^{-1} \hat{\sigma}_1$, with $\hat{\sigma}_1 = \text{median}(\|\mathbf{w}_1 - \text{median}(\mathbf{w}_1)\|)/0.6745$ [4]. The s.d. at other scales $\{\hat{\sigma}_j\}$ can be obtained by relation (9) with $\sigma = \hat{\sigma}$. The significant coefficients can then be obtained as in classical denoising by τ_j -thresholding, where τ_j is typically in the range $[3\hat{\sigma}_j \ 5\hat{\sigma}_j]$. The resulting set of non zero coefficients can be stored in a vector $\tilde{\mathbf{m}}$. The second step accounts for convolution. In radiointerferometry, the PSF has a large number of sidelobes (e.g. Fig.4, top right). The information related to one object is consequently spread very far over the data image, while being in the same time contaminated by other objects' contribution and by noise. Since we wish to detect compact bright structures first, we want to focus at each step on the main lobe of the brightest object. Consequently, we further threshold

the coefficients of $\tilde{\mathbf{m}}$ at each scale j using a threshold proportional to the maximum $|w^{m,j}|$ of the coefficients of $\tilde{\mathbf{m}}$ at scale j (a threshold value of $|w^{m,j}|/2$ was used in the simulations below). The brightest object is then likely to have a good fraction of its coefficients among the resulting set of non zero coefficients. This set can be stored in a vector \mathbf{m} , whose support is the SAS. The next question is to determine which coefficients in \mathbf{m} actually correspond to the brightest object.

• *Objects extraction:* We need a few definitions here, adapted from [6]. A *structure* is defined as a set of connected (contiguous) nonzero analysis coefficients of the same scale j . An *object* will be characterized by a set of structures of different levels that are connected in a sense specified below.

We first identify the brightest structure and its level j^m as the structure in the SAS containing the maximum analysis coefficient $|w^{m,j}|$. This structure, \mathbf{s}_{j^m} , is associated to the brightest object. Then, the other structures of this object are searched only at scales ($j = 1, \dots, j^m - 1$), as information of bright compact objects will still be present at higher frequencies. For instance, the small galaxy at the bottom right of Fig.2 has its maximum in \mathbf{w}_4 , but still presents relatively large coefficient in \mathbf{w}_2 and \mathbf{w}_3 . Then, the structure \mathbf{s}_{j^m} of scale j^m will be connected to the brightest structure \mathbf{s}_{j^m-1} of scale $j^m - 1$ if the spatial position of the maximum wavelet coefficient $|w^{m,j}|$ in scale j^m also belongs to the brightest structure \mathbf{s}_{j^m-1} in scale $j^m - 1$. If this is the case the process is repeated between \mathbf{s}_{j^m-1} and \mathbf{s}_{j^m-2} , and so on. Otherwise, the process stops. The resulting set of connected structures constitute the significant coefficients identifying the signature of the brightest object in the data. These coefficients are stored in a sparse vector $\boldsymbol{\alpha}$ of dimension $(N(J+1), 1)$.

3.2. Algorithm

These ideas lead to the following analysis-by-synthesis algorithm:

• **Initialization:** Major iteration index $i = 0$. Initial residual $\mathbf{r}_0 = \mathbf{y}$ and solution $\hat{\mathbf{x}}_0 = \mathbf{0}$. Determine $\boldsymbol{\alpha}_0$ corresponding to the brightest object in \mathbf{r}_0 as in Sec. (3.1).

• **While $\boldsymbol{\alpha}_i \neq \mathbf{0}$:**

– **Analysis based deconvolution:** Estimate $\hat{\mathbf{X}}_{i+1}$ by solving:

$$\hat{\mathbf{X}}_{i+1} = \arg \min_{\mathbf{z}} \|\boldsymbol{\alpha}_i - \mathcal{P}_{\boldsymbol{\alpha}_i}(\mathbf{A}^T \mathbf{H} \mathbf{z})\|^2, \quad (10)$$

where $\mathcal{P}_{\boldsymbol{\alpha}_i}(\mathbf{A}^T \mathbf{H} \mathbf{z})[k] = 0$ if $\boldsymbol{\alpha}_i[k] = 0$, and $\mathcal{P}_{\boldsymbol{\alpha}_i}(\mathbf{A}^T \mathbf{H} \mathbf{z})[k] = (\mathbf{A}^T \mathbf{z})[k]$ otherwise. An efficient way to solve this problem is to use the iterative (minor iteration index (k)) projected Van Cittert scheme [6]:

$$\hat{\mathbf{X}}_{i+1}^{(k+1)} = \mathcal{P}^+(\hat{\mathbf{X}}_{i+1}^{(k)} + \mathbf{S}(\boldsymbol{\alpha}_i - \mathcal{P}_{\boldsymbol{\alpha}_i}(\mathbf{A}^T \mathbf{H} \hat{\mathbf{X}}_{i+1}^{(k)}))), \quad (11)$$

where \mathcal{P}^+ is the projector on the positive orthant. The initial $\hat{\mathbf{X}}_{i+1}^{(0)}$ is obtained by applying the reconstruction scheme (6) on $\mathcal{P}_{\boldsymbol{\alpha}_i}(\mathbf{A}^T \mathbf{r}_i)$ instead of \mathbf{a} in (6). Iterations (11) stop if $\frac{\|\hat{\mathbf{X}}_{i+1}^{(k+1)} - \hat{\mathbf{X}}_{i+1}^{(k)}\|_2^2}{\|\hat{\mathbf{X}}_{i+1}^{(k)}\|_2^2}$ does not change significantly (less than 1%

in the results below), in which case we set $\hat{\mathbf{X}}_{i+1} = \hat{\mathbf{X}}_{i+1}^{(k+1)}$.

– **Synthesis step:**

○ $\hat{\mathbf{x}}_{i+1} = \hat{\mathbf{x}}_i + \hat{\mathbf{X}}_{i+1} = \hat{\mathbf{X}} \mathbf{1}_{i+1}$, $\hat{\mathbf{X}} = [\hat{\mathbf{X}}_1, \dots, \hat{\mathbf{X}}_{i+1}]$.

○ $\mathbf{r}_{i+1} = \mathbf{r}_i - \mathbf{H} \hat{\mathbf{X}}_{i+1}$.

○ Determine $\boldsymbol{\alpha}_{i+1}$ corresponding to the brightest object in \mathbf{r}_{i+1} as in Sec. (3.1), and set $i = i + 1$.

• **End.**

The number of deconvolved objects P is the iteration number when the algorithm stops, and the restored image is $\hat{\mathbf{x}} = \hat{\mathbf{X}} \mathbf{1}_P$.

4. RESULTS AND DISCUSSION

Results are given in this section for a simulated image \mathbf{x} ($N = 512^2$, Fig. 4, top left) which contains two compact, bright objects \mathbf{X}_1 and \mathbf{X}_2 (of maximum intensity 255, see the zooms in Fig. 3, top row) and a diffuse, fainter source \mathbf{X}_3 . As a comparison method, we have opted for ISRA (Image Space Reconstruction Algorithm, [4]), which in Astronomy is an efficient and widely used Maximum Likelihood method under Gaussian noise with positivity constraint. ISRA has however two drawbacks: first, the number of iterations that yield best reconstruction can not be known; second, ISRA can not deal with negative PSFs, as the ones encountered for ASKAP radiointerferometer for instance. Thus, to compare with the proposed method, we first used a positive convolution kernel (B-spline of order 3). ISRA at best reconstruction is used for reference. We also show the results of a state-of-the-art method, an IUWT-regularized version of ISRA, which has a natural stopping criterion and whose iterative scheme is [6, 7]: $\mathbf{x}^{(k+1)} = \text{diag}(\mathbf{x}_i^{(k)}) \left[\frac{\mathbf{H}^T (\mathbf{H}\mathbf{x}^{(k)} + \mathbf{S}(\mathcal{T}_{\tau_j}(\mathbf{A}^T \mathbf{r}^{(k)})))}{\mathbf{H}^T \mathbf{H}\mathbf{x}^{(k)}} \right]$, where $\mathbf{r}^{(k)} = \mathbf{y} - \mathbf{H}\mathbf{x}^{(k)}$, \mathcal{T}_{τ_j} denotes the hard-thresholding operator used on the IUWT-analysis coefficients of $\mathbf{r}^{(k)}$ ($\tau_j = 5\sigma_j$).

The results with the positive convolution kernel are shown in Fig. 3. In this test the Gaussian noise added to the convolved data has $\sigma = 10$, which is 5 times higher than the faint source \mathbf{X}_3 ($\|\mathbf{X}_3\|_\infty = 2$). The criterion to compare how well $\hat{\mathbf{x}}$ approximates \mathbf{x} is the SNR ($\text{SNR}(\mathbf{x}, \hat{\mathbf{x}}) = 10 \log_{10} \frac{\|\mathbf{x}\|^2}{\|\mathbf{x} - \hat{\mathbf{x}}\|^2}$). The ISRA yields at best reconstruction a SNR of 18.7 dB (after 10 iterations, image not displayed). IUWT-regularized ISRA yields a SNR of 18.1 dB (Fig. 3, bottom row), and the proposed method a SNR of 20.2 dB (Fig. 3, middle row). Note that the faint component is not recovered by IUWT-regularized ISRA (nor by ISRA), and varying τ_j in the range $[3\sigma_j \dots 5\sigma_j]$ did not yield noticeable improvement. The "source" visible in the zoomed region shown in Fig. 3, lower right corner, is only caused by the saturation of the restituted bright components on the $[0 \ 2]$ flux scale. These results show that the proposed method is very efficient to recover and extract the faint source, and also that there may be room for improvement in estimating the bright sources. Our method allows to recover the sources componentwise, and to evaluate a SNR per source (20.2 dB for \mathbf{X}_1 , 14.7 dB for \mathbf{X}_2 and 11.7 dB for \mathbf{X}_3 here), which is not the case of regularized-ISRA.

The second results (Fig. 4) deal with a PSF similar to ASKAP radiointerferometer (top, right). The dirty map \mathbf{y} (top, middle) obtained with this PSF has a SNR of 6.5 dB. Here $\sigma = 1$, but the faint source ($\|\mathbf{X}_3\|_\infty = 8$ here) is totally buried in the replica of the bright sources because of the PSF sidelobes. The proposed method yields a solution $\hat{\mathbf{x}}$ with SNR= 15.7dB. The faint source (middle row, right) is very well restored (SNR= 17.7dB). From Fig.4, bottom row, we can see the evolution of the residual \mathbf{r}_i after successive subtractions of components $\mathbf{H}\hat{\mathbf{X}}_i$. The faint diffuse source, initially invisible in \mathbf{y} , appears clearly after subtraction of the bright sources. The final residual is very similar to noise, confirming that the information has efficiently been extracted. The whole process takes a few minutes on a laptop.

5. CONCLUSIONS

The proposed deconvolution method uses sparse priors in an iterative analysis-by-synthesis manner with IUWT dictionaries. The restored image is the sum of deconvolved sources which can be studied independently. The presented results show that the method is efficient to recover faint sources initially buried in bright sources' contributions, and it is fast. A modeling effort is needed to better identify the analysis coefficients of bright sources. The adaptation of the method to sources with irregular morphologies is also under investigation.

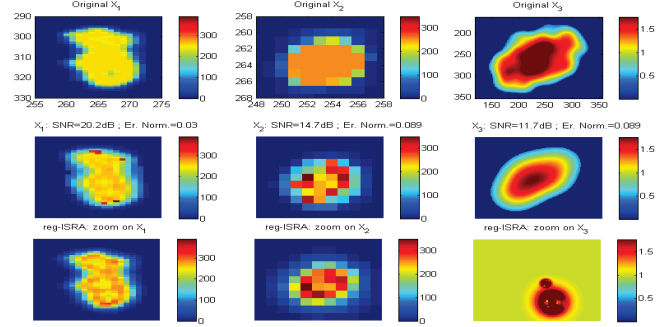


Fig. 3. From top to bottom: objects (\mathbf{X}_i) composing the image \mathbf{x} of Fig. 4 top left ; estimated objects by the proposed approach; zoom on the corresponding regions of the IUWT-regularized ISRA solution.

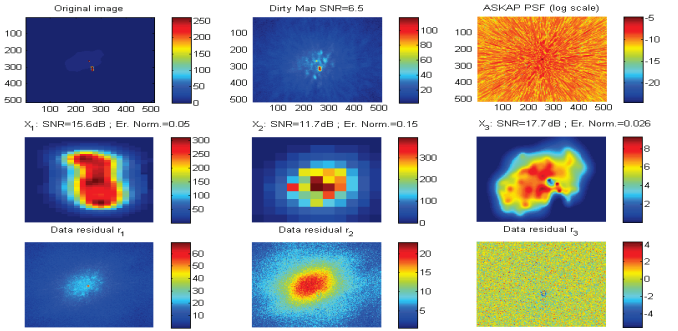


Fig. 4. From left to right : Top row : Image $\mathbf{x} = \mathbf{X}_1 + \mathbf{X}_2 + \mathbf{X}_3$, data \mathbf{y} , ASKAP-like PSF (log scale). Middle row: reconstructed components (same pixel regions as in Fig. 3 are shown). Bottom row: residual data \mathbf{r}_1 , \mathbf{r}_2 and \mathbf{r}_3 after successive subtractions of $\mathbf{H}\hat{\mathbf{X}}_1$, $\mathbf{H}\hat{\mathbf{X}}_2$, $\mathbf{H}\hat{\mathbf{X}}_3$. The faint source appears in \mathbf{r}_2 , \mathbf{r}_3 is close to noise.

6. REFERENCES

- [1] U. Rau, S. Bhatnagar, M.A. Voronkov, and J.T. Cornwell, "Advances in calibration and imaging techniques in radio interferometry," in *Proc. of the IEEE*, 2009, vol. 97, pp. 1472–1481.
- [2] M. Elad, P. Milanfar, and R. Rubinstein, "Analysis versus synthesis in signal priors," *Inverse Problems*, vol. 23, no. 3, pp. 947–968, 2007.
- [3] J.A. Högbom, "Aperture synthesis with a non-regular distribution of interferometer baselines," *Astron. Astrophys. Suppl.*, vol. 15, pp. 417–426, 1974.
- [4] J.-L. Starck, F. Murtagh, and J.M. Fadili, *Sparse Image and Signal Processing: Wavelets, Curvelets, Morphological Diversity*, pp. 45–64, 122–123, Cambridge University Press, 2010.
- [5] A. Bijaoui, J.-L. Starck, and F. Murtagh, "Restauration des images multi-échelles par l'algorithme à trous," *Traitement du Signal*, vol. 11, no. 3, pp. 229–243, 1994.
- [6] J.-L. Starck, F. Murtagh, and M. Bertero, *Starlet Transform in Astronomical Data Processing: Application to Source Detection and Image Deconvolution*, Springer, 2011.
- [7] J.-L. Starck, F. Murtagh, and A. Bijaoui, "Multiresolution support applied to image filtering and restoration," *Graphical Models and Image Processing*, vol. 57, no. 5, pp. 420 – 431, 1995.